Electronic Supplementary Material (ESI) for New Journal of Chemistry.

Multifunctional $Fe_3O_4/TiO_2/NH_2$-UiO-66 with integrated interfacial features for favorable phosphate adsorption

Liyu Yang †[a], Shangui Zhang †[b], Xiangcheng Shan [a], Chang-sik Ha [c], Qingda An [a,], Zuoyi Xiao [a], Li Wei *[a] , Shangru Zhai *[a]

[a] *Liaoning Key Lab of Lignocellulose Chemistry and BioMaterials, Liaoning Collaborative Innovation Center for Lignocellulosic Biorefinery, College of Light Industry and Chemical Engineering, Dalian Polytechnic University, Dalian 116034, China*

[b] *Marine Chemical Research Institute Co., Ltd., Qingdao 266071, China ;State Key Laboratory of Marine Coatings*

[c] *Department of Polymer Science and Engineering, Pusan National University, Republic of Korea*

† *Their contributed equally to this work*

***Corresponding author**

Tel.: (+86) 411-8632-3649; Fax: (+86) 411-8632-364679

E-mail address: lucy_weili@163.com; zhaisrchem@163.com

1. Supporting texts

Text S1. Materials

$FeCl_3·6H_2O$, CH_3COONa (NaAC), Ethylene glycol ($C_2H_6O_2$), Acetonitrile (CH_3CN), Acetone (CH_3COCH_3), NaOH (AR, ≥96.0%), Acetic acid (CH_3COOH), Ammonia solution (NH_3, AR, 25%) and N,N-dimethylformamide (DMF) were purchased from Tianjin Kermel Chemical Reagent Co., Ltd., Zirconium(IV) chloride ($ZrCl_4$) and 2-Aminoterephthalic acid (H_2ATA, $C_8H_7NO_4$) were provided by Macklin, Polyethylene glycol (PEG, $HO(CH_2CH_2O)_nH$, average Mn 4000) was purchased from Aladdin Reagent, Ethanol (CH_3CH_2OH, AR, ≥99.7%) and KH_2PO_4 were provided by Tianjin Fuyu Fine Chemical Co., Ltd., Hydrochloric acid (HCl, GR, 36.0~38.0%), Cetyltrimethylammonium bromide (CTAB, $C_{19}H_{42}BrN$, 99.0%) and Tetra-n-butyl titanate (TBOT, $C_{16}H_{36}O_4Ti$, CP, ≥98.0%) were provided by Sinopharm Chemical ReagentCo. All chemical reagents are used directly in the absence further processing.

Text S2.1 Synthesis of Fe_3O_4

2.5 g of $FeCl_3·6H_2O$, 7.2 g of NaAC and 2 g of PEG were mixed with 80 mL of Ethylene glycol. After continuous stirring until it was completely dissolved, it was added to a 100 mL Teflon autoclave and reacted at 200 °C for 8 h. After its temperature drops to 25 °C, it is separated by an applied magnetic field, rinsed with deionized water (DW) and ethanol three times, respectively. And freeze-dried for 12 h.

Text S2.2 Synthesis of TiO_2

4 mL of tetrabutyl titanate was dissolved in 60 mL of acetone, and after magnetic

stirring at 25 °C for 30 min, it was transferred to a 100 mL Teflon reaction kettle. The reaction was carried out at 180 °C for 12 h. After cooling to room temperature, suction filtration and washing with ethanol three times, and then drying in a vacuum drying oven at 80 °C overnight. The dried samples were heated to 200 °C at a rate of 5 °C/min and held for 2 h in a muffle furnace to obtain TiO_2.

Text S2.2 Synthesis of NH_2-UiO-66

Add 0.2 g of $ZrCl_4$ and 0.156 g of H_2ATA to 30 mL of DMF in an ultrasonic environment, respectively. Then make it evenly dispersed for 30 min. The mixture was transferred to a 100 mL polytetrafluoroethylene reaction kettle, and reacted in an oven at 120 °C for 24 h. After cooling to room temperature, the samples were washed three times with ethanol and DMF, respectively. Finally, it was dried overnight in a vacuum drying oven at 80 °C to obtain NH_2-UiO-66.

Text S3. Details of characterizations

The morphology of $Fe_3O_4/TiO_2/NH_2$-UiO-66 was observed utilizing transmission/scanning electron microscope (TEM; JEM, Japan)/(SEM, JEOL, Japan) and the elemental composition and content were analyzed by energy spectrometer (EDS, Oxford, UK). Fourier transform infrared spectra (FT-IR, 5700, Nicolet, USA) was used to study the functional groups of adsorbents. Crystallization properties of materials were investigated by X-ray diffractometer (XRD, 7000S, Japan). The N_2 adsorption-desorption isotherms and specific surface area were described by Brunauer-Emmett-Teller (BET) method at 77 K via JW-BK222 analyzer. The

adsorption mechanism of phosphate was studied by X-ray photoelectron spectrum (XPS, ESCALAB250, Thermo VG, USA) and Zeta potentials (3000HSA, UK). The concentration of residual phosphorus after adsorption was determined by molybdenum blue spectrophotometry with UV-Vis spectrophotometer (UV-754N Shanghai, China). Thermogravimetric analysis (TGA) and differential thermogravimetric (DTG) were studied with TG the temperature spectrum from 30 to 800 °C at a rate of 5 °C/min under nitrogen. The magnetic field intensity of magnetite before and after adsorption was measured using a vibrating sample magnetometer (VSM, Lake shore 7400). The content of Fe, Ti and Zr in the solution after phosphate adsorption was measured by ICP-MS (Samefi, USA).

Text S4. Details of Fig S1.

The effects of $Fe_3O_4/TiO_2/NH_2$-UiO-66 adsorbents synthesized with different mass ratios of Fe_3O_4/TiO_2 and $ZrCl_4$ on the phosphate adsorption performance were investigated through preliminary evaluation experiments. 20 mg of adsorbents in different ratios were added to 20 mL of phosphate solution with an initial concentration of 100 mg/L, and the experimental results obtained after 24 h of static adsorption are shown in **Fig. S1.** When the mass ratio of Fe_3O_4/TiO_2 to $ZrCl_4$ is 1:2, the adsorption capacity is in the optimal state, so this ratio of adsorbents will be used in subsequent experiments.

Text S5. Elemental composition analysis

From the comparison of Fig S(2, 3), it can be seen that the peak of P element

85 appears in the spectrum after adsorption, which corresponds to the elements in Table
86 S(1, 2). After adsorption, the content of O element increased from 44.16wt% to
87 47.89wt%, and the content of P element was 1.23wt%, which proved the successful
88 adsorption of phosphate.

89 **Text S6. Adsorption isotherms models**

90 Langmuir model:

$$q_e = \frac{q_m K_L C_e}{1 + K_L C_e} \tag{S1}$$

91

92 Freundlich model:

$$q_e = K_F C_e^{\frac{1}{n}} \tag{S2}$$

93

94 where K_F (mg/g) and n are two empirical constants of Freundlich model, q_m (mg/g) is
95 the maximum adsorption capacity of phosphate, q_e (mg/g) is the adsorption capacities
96 at adsorption equilibrium, C_e (mg/L) is the concentration of residual phosphate
97 solution after adsorption. K_L (L/mg) is the Langmuir constant.

98 **Text S7. Adsorption kinetics models**

99 Pseudo-first-order model (PFO) :

$$\ln(q_e - q_t) = lnq_e - K_1 t \tag{S3}$$

100

101 Pseudo-second-order model (PSO) :

$$\frac{t}{q_t} = \frac{1}{K_2 q_e^2} + \frac{t}{q_e} \tag{S4}$$

102

103 Intraparticle diffusion model:

$$q_t = k_i t^{0.5} + \theta \tag{S5}$$

104

105

106 where q_e (mg/g) and q_t (mg/g) are the adsorption capacities at adsorption equilibrium

and at time t (min), and K_1 (min^{-1}) and K_2 (g/(mg·min)) are the rate constants. k_i (mg/g·$min^{-1/2}$)) and θ were the intercepts of diffusion coefficient and internal diffusion model, respectively.

Text S8. Competitive adsorption of coexisting anionic ions.

$$K_d = \frac{(C_0 - C_e)}{C_e} \times \frac{V}{m} \quad \text{(S6)}$$

where K_d is the distribution coefficient.

Text S9. Adsorption thermodynamics

The thermodynamic parameters of $Fe_3O_4/TiO_2/NH_2$-UiO-66 adsorption of phosphate including Gibbs free energy ΔG^0 (kJ/mol), entropy change ΔS^0 (J/mol·K) and enthalpy change ΔH^0 (kJ/mol) were calculated by the following equations (Equations S(7)-(10)):

$$\Delta G^0 = \Delta H^0 - T\Delta S^0 \quad \text{(S7)}$$

$$lnK_d = \frac{\Delta S^0}{R} - \frac{\Delta H^0}{RT} \quad \text{(S8)}$$

$$\Delta G^0 = -RTlnK_d \quad \text{(S9)}$$

$$K_d = \frac{q_e}{C_e} \quad \text{(S10)}$$

where R is the ideal gas constant (J/mol·K) and T is the absolute temperature (K); K_d is the adsorption thermodynamic equilibrium constant; q_e (mg/g) is the adsorption capacities at adsorption equilibrium; C_e (mg/L) is the concentration of residual phosphate solution after adsorption.

Text S10. Calculation method

To gain a more detailed understanding of the adsorption mechanism and

configuration of $Fe_3O_4/TiO_2/NH_2$-UiO-66 on phosphate, DFT calculations were performed. Since the contribution of NH_2-UiO-66 in the whole adsorbent is relatively large, NH_2-UiO-66 is selected for the calculation study. Using the DMol3 code in the Materials studio software, the results of the adsorption experiment were theoretically described, and the phosphate adsorption mechanism was further explained. First-principles studies are based on the generalized gradient approximation (GGA) and the Perdew-Burke-Ernzerhof (PBE) methods. The formula for calculating the adsorption energy (E_{ads}) between the adsorbent molecule and phosphate is as follows:

$$E_{ads}=E(total)-E(adsorbent)-E(phosphate) \quad (S11)$$

where E(total), E(adsorbent) and E(phosphate) are the total energies of the adsorbed system, the adsorbent molecule and one energy of phosphate, respectively.

2. Supporting Figures and Tables

Fig S1. Preliminary evaluation of adsorbents with different ratios of Fe_3O_4/TiO_2 and $ZrCl_4$.

Fig S2. EDS spectrum of $Fe_3O_4/TiO_2/NH_2$-UiO-66 before phosphate adsorption.

Fig S3. EDS spectrum of $Fe_3O_4/TiO_2/NH_2$-UiO-66 after phosphate adsorption.

Fig S4. Nitrogen adsorption-desorption curves of (a) Fe_3O_4; (b) TiO_2; (c) NH_2-UiO-66; (d) Fe_3O_4/TiO_2; (e) $Fe_3O_4/TiO_2/NH_2$-UiO-66; (f) $Fe_3O_4/TiO_2/NH_2$-UiO-66-P.

Fig S5. Pore size distributions of (a) Fe_3O_4; (b) TiO_2; (c) NH_2-UiO-66; (d) Fe_3O_4/TiO_2; (e) $Fe_3O_4/TiO_2/NH_2$-UiO-66; (f) $Fe_3O_4/TiO_2/NH_2$-UiO-66-P.

Fig S6. TG-DTG curves of $Fe_3O_4/TiO_2/NH_2$-UiO-66.

Fig S7. Magnetization curves of Fe_3O_4, $Fe_3O_4/TiO_2/NH_2$-UiO-66 and $Fe_3O_4/TiO_2/NH_2$-UiO-66-P.

Fig S8. Effect of dosage on phosphate adsorption capacity.

Fig S9. (a) Effect of temperature on phosphate adsorption; (b) The point-line graph of $\ln K_d$ and 1/T.

Table S1. Element ratios of $Fe_3O_4/TiO_2/NH_2$-UiO-66 before phosphate adsorption.

Table S2. Element ratios of $Fe_3O_4/TiO_2/NH_2$-UiO-66 after phosphate adsorption.

Table S3. Kinetic arguments of the phosphate adsorption process.

Table S4. The thermodynamic parameters of $Fe_3O_4/TiO_2/NH_2$-UiO-66.

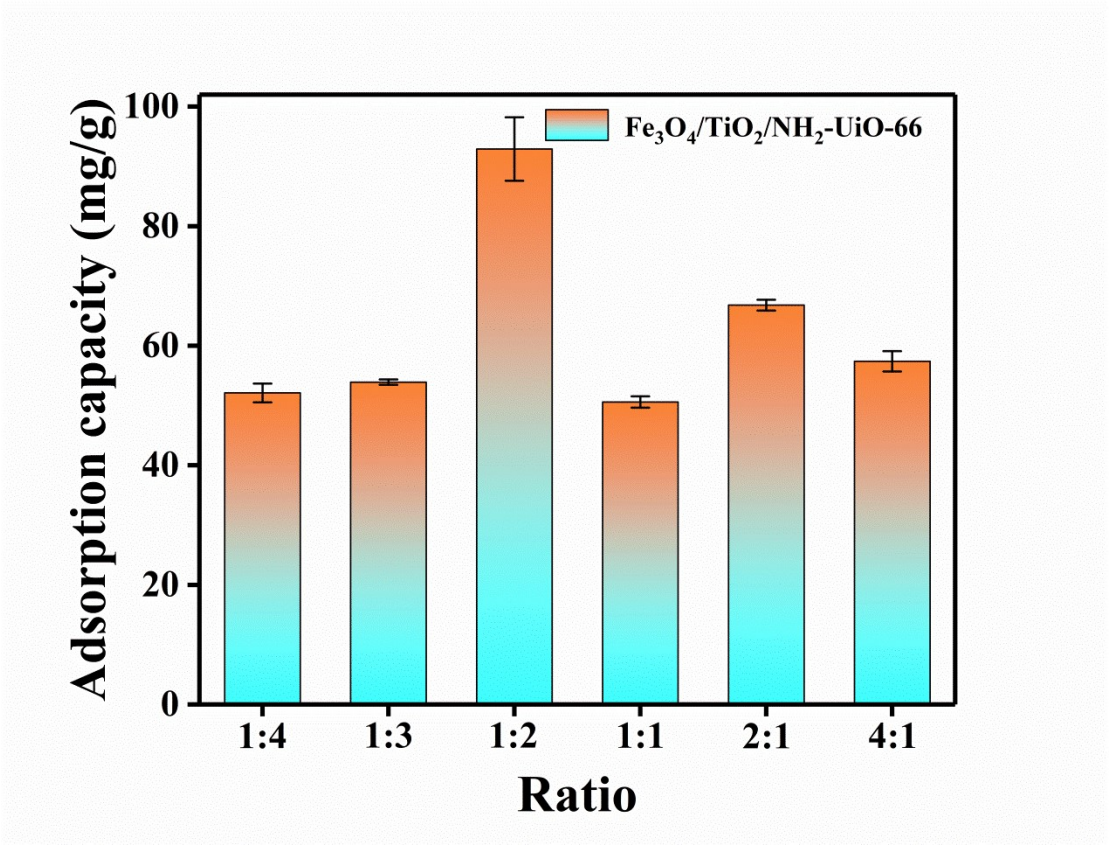

158

159 **Fig S1.**

160

161

162

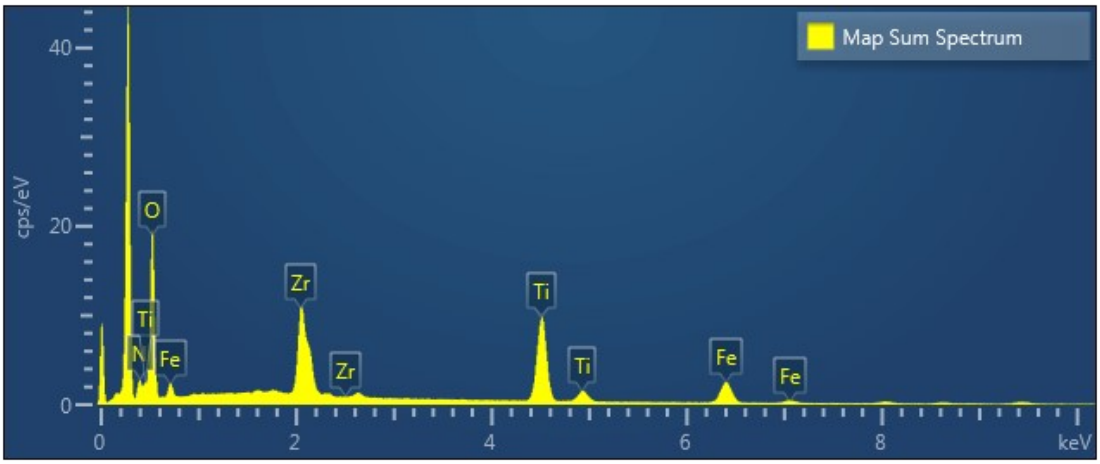
Map Sum Spectrum
cps/eV
40
20
0
O
Ti
N
Fe
Zr
Zr
Ti
Ti
Fe
Fe
0
2
4
6
8
keV

Fig S2.

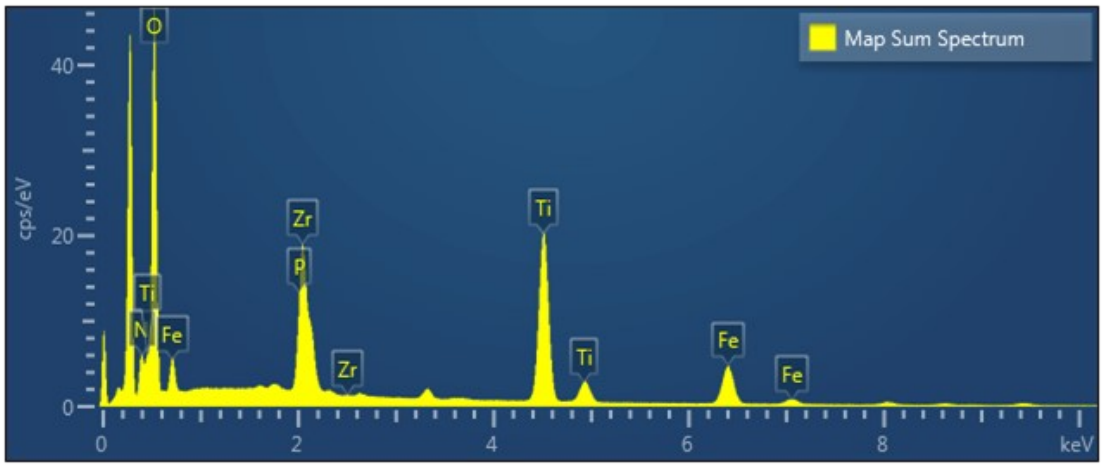
Map Sum Spectrum
cps/eV
40
20
0
O
Ti
N
Fe
Zr
P
Zr
Ti
Ti
Fe
Fe
0
2
4
6
8
keV

Fig S3.

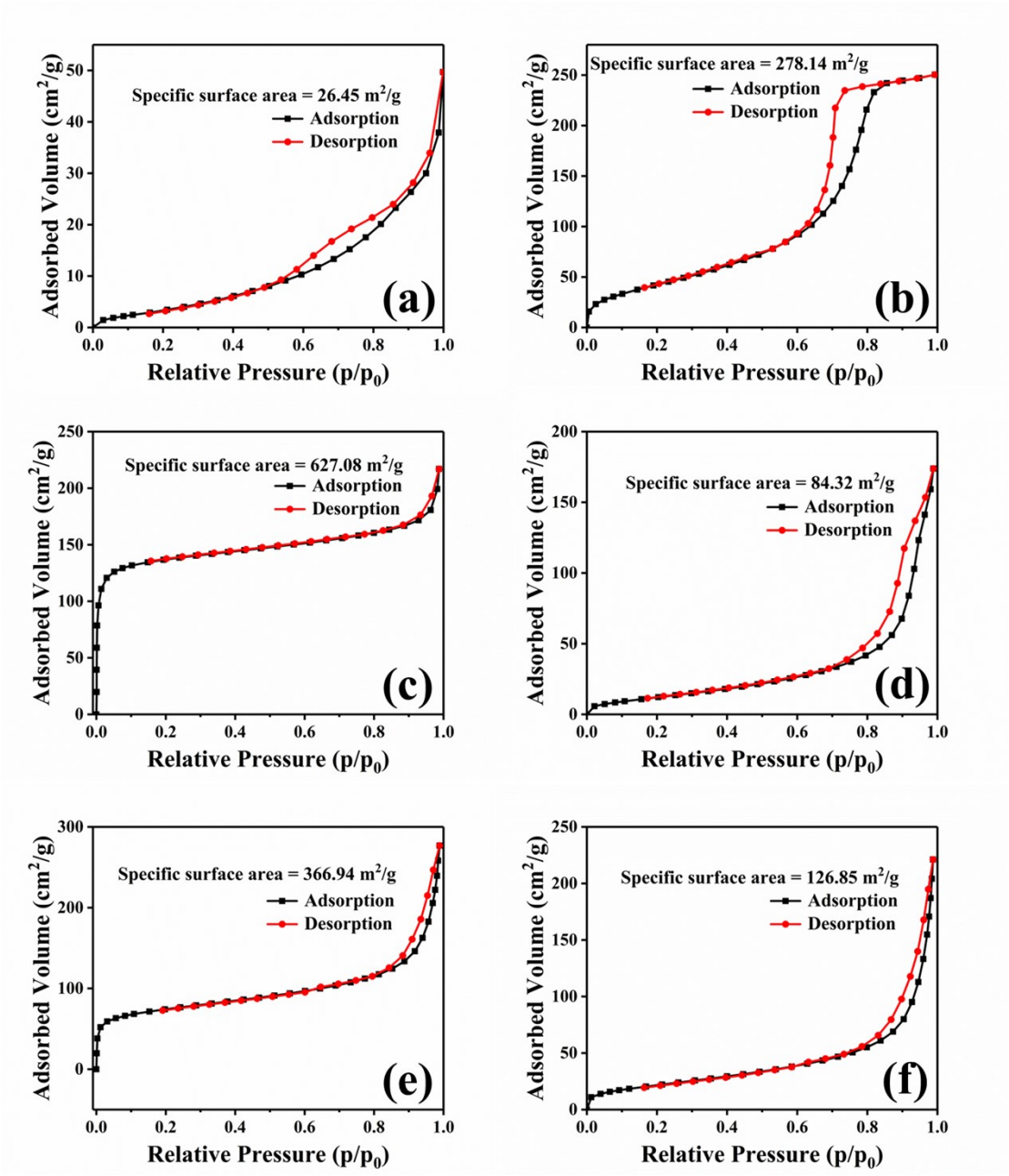

172

173 **Fig S4.**

174

175

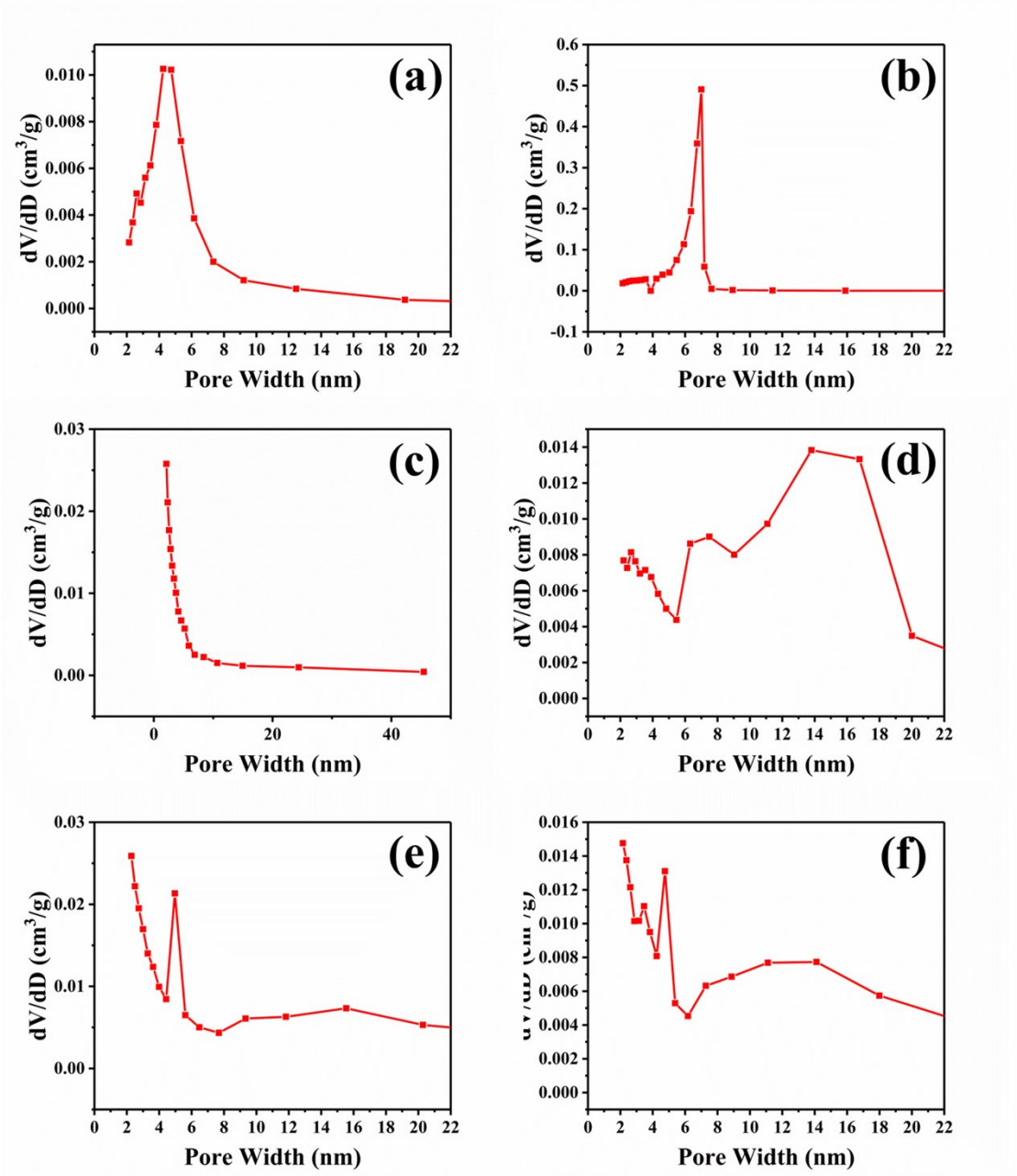

176

177 **Fig S5.**

178

179

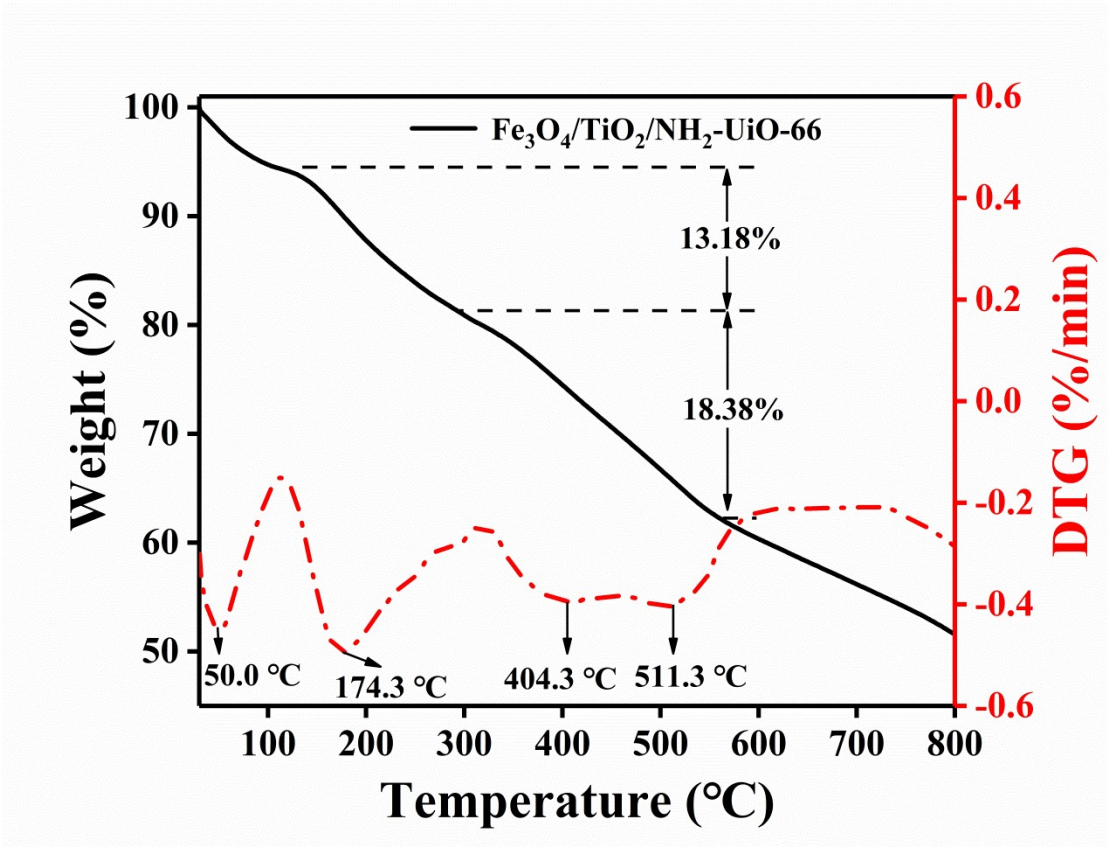
Fe3O4/TiO2/NH2-UiO-66
13.18%
18.38%
50.0 °C
174.3 °C
404.3 °C
511.3 °C
Weight (%)
DTG (%/min)
Temperature (°C)
100
90
80
70
60
50
0.6
0.4
0.2
0.0
-0.2
-0.4
-0.6
100
200
300
400
500
600
700
800

Fig. S6

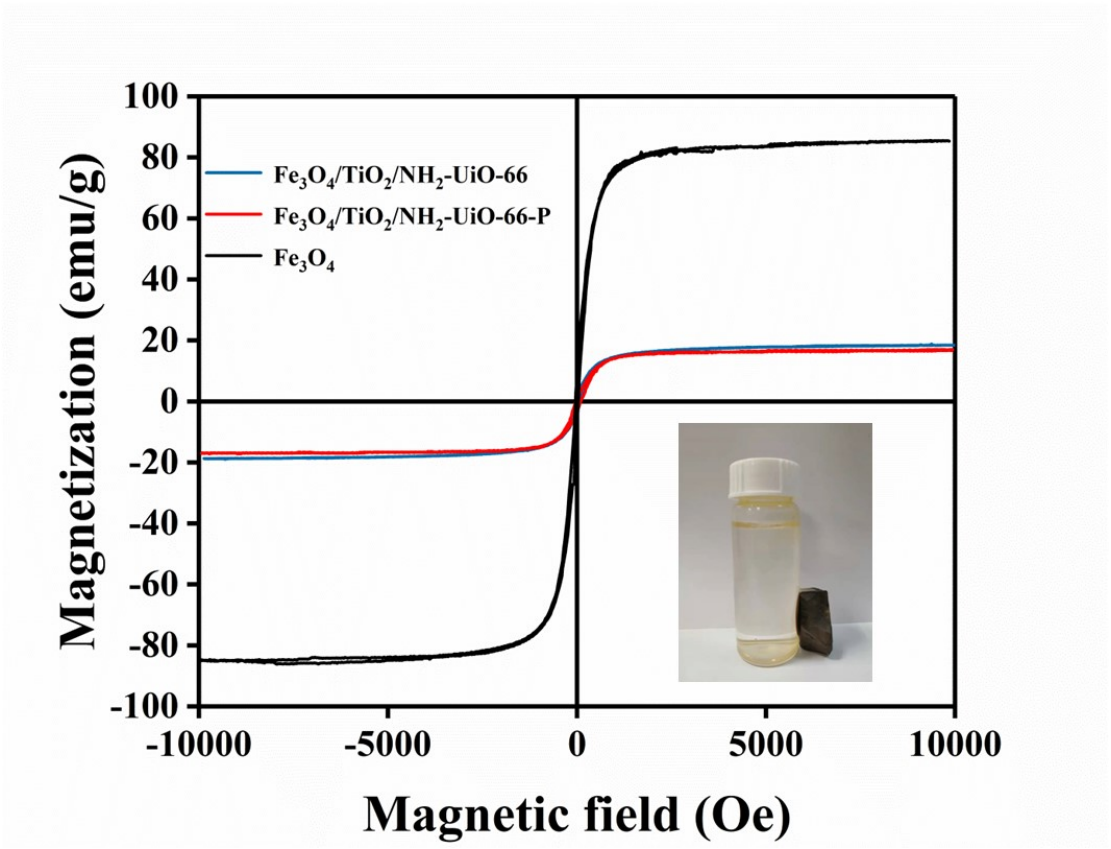

184

185 **Fig S7**

186

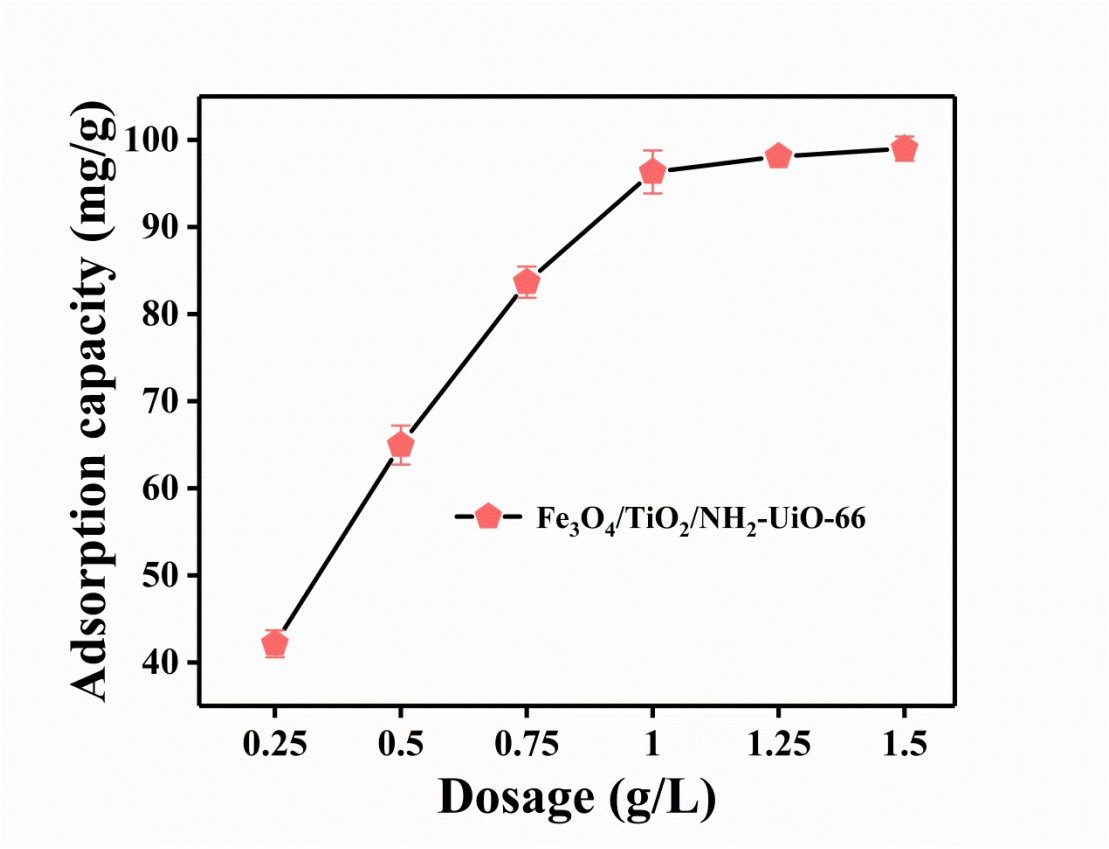
Adsorption capacity (mg/g)
100
90
80
70
60
50
40
0.25
0.5
0.75
1
1.25
1.5
Dosage (g/L)
Fe3O4/TiO2/NH2-UiO-66

Fig S8.

191

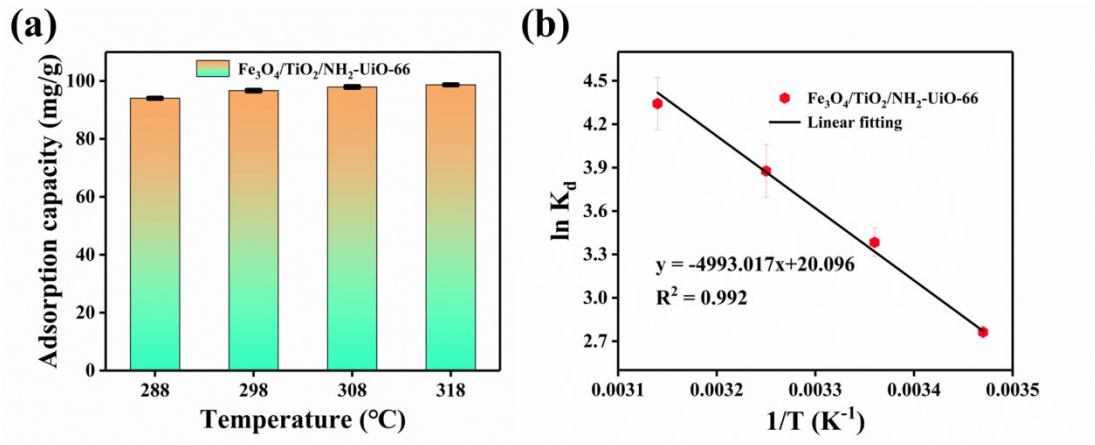

192

193 **Fig S9.**

194

195

196 **Table S1.**

197

Element	Line Type	Apparent Concentration	k Ratio	Wt%
N	K series	1.69	0.00302	1.81
O	K series	15.71	0.05813	42.36
Ti	K series	12.09	0.12091	23.33
Fe	K series	6.88	0.06882	13.52
Zr	L series	8.75	0.08746	18.98
Total:				100.00

198

199

Table S2.

Element	Line Type	Apparent Concentration	k Ratio	Wt%
N	K series	1.35	0.00263	1.14
O	K series	23.16	0.08409	44.39
P	K series	1.98	0.00744	1.83
Ti	K series	15.67	0.15670	23.75
Fe	K series	8.19	0.08195	12.74
Zr	L series	9.45	0.08414	16.15
Total:				100.00

205 **Table S3.**

206

	Pseudo-first-order model			Pesudo-second-order model		
	q_e (mg/g)	k_1 (1/min)	R^2	q_e (mg/g)	k_2 (g/(mg·min))	R^2
100 mg/L	79.954	0.0872	0.730	83.294	0.0020	0.981
200 mg/L	148.201	0.0431	0.815	157.746	0.0005	0.975

207

208 **Table S4.**

209

T (K)	K_d	Ln (K_d)	$\triangle G^0$ (KJ/mol)	$\triangle H^0$ (KJ/mol)	$\triangle S^0$ (J/mol·K)	R^2
288	15.847	2.763	-6.616			
298	29.459	3.383	-8.382	41.512	167.078	0.992
308	48.279	3.877	-9.928			
318	76.938	4.343	-11.482			

210